Ultrasonic waves in multilayered superconducting plates

Ernian Pan and Subhendu K. Datta
Department of Mechanical Engineering, University of Colorado, Boulder, Colorado 80309

(Received 8 October 1998; accepted for publication 23 March 1999)

Guided waves and the transient response of multilayered superconducting tapes have been studied in this article. These tapes are usually composed of layers of a superconducting material (like $YBa_2Cu_3O_{7-\delta}$, or YBCO, for simplicity) alternating between layers of a metallic material (like nickel or silver). The tapes are thin, the thickness being in the range of 100–200 μm. The superconducting layer is orthotropic with a thickness of 5–10 μm. In applications, the tapes are long and have a finite width. In this article, we focus our attention on the dispersion of two-dimensional guided waves and the transient response of homogeneous and three-layered tapes assuming that the thickness of the superconducting layer is much smaller than the metal layer. Three tape geometries are considered: a homogeneous nickel layer, a three-layered YBCO/nickel/YBCO and a three-layered nickel/YBCO/nickel. It is found that although the total thickness of the YBCO layer is very small, the dispersion and transient response in the last two cases are quite different from each other and from the homogeneous nickel plate. These differences can be used for the ultrasonic characterization of the in-plane material properties of the superconducting layers. © *1999 American Institute of Physics.* [S0021-8979(99)02613-4]

I. INTRODUCTION

The ultrasonic nondestructive evaluation (NDE) technique has found wide use for quantitative characterization of mechanical properties and for detection of cracks and delaminations in laminates. In using this method, however, one needs to have a clear understanding of wave propagation in anisotropic and layered plates. For complex wave interaction phenomenon occurring in the damaged layered system, a general analytical solution is extremely difficult, if not impossible, to obtain. This necessitates the use of numerical methods, such as the finite-element method (FEM) or the boundary-element method (BEM). It is noted, however, that the latter is more suited than the former to cases where better accuracy is required due to problems such as stress concentration or where the domain of interest extends to infinity.

In applying the BEM formulation to the layered plate, one needs to find the Green's functions in such a system. The two-dimensional (2D) elastodynamic Green's functions due to line sources in a layered system were studied previously by Kundu and Mal,[1] Mal,[2] and Ju[3] employing the propagator matrix method. A thin-layer method was also proposed for the solution of the Green's functions in two dimensions.[4,5] More recently, Zhu, Shah, and Datta[6,7] and Zhu and Shah[8] derived these Green's functions using a stiffness method combined with either a wave-function expansion or a modal summation technique. Similarly, Liu and Achenbach[9] obtained the Green's function using a strip-element method.

This article presents an alternative and accurate method to calculate the 2D elastodynamic Green's functions in anisotropic and layered plates. It is an extension of the modal summation technique used by Zhu, Shah, and Datta[6] and Liu and Achenbach.[9] As in the modal summation technique, we first divide the layered system into a certain number of thin layers and use the stiffness method[10] to find approximately the wave numbers (including not only the propagating modes, but also the nonpropagating and evanescent modes). Then, we use the exact dispersion equation,[11] which is obtained with a direct propagator matrix method,[12] to find the wave numbers accurately. Finally, the direct propagator matrix method and the modal summation technique (Cauchy's residue theorem) are used to derive the frequency-domain Green's functions. The time-domain Green's functions are obtained by the inverse Fourier transformation combined with an exponential window method.[9,13,14]

This general technique for analyzing the Green's functions in anisotropic and layered plates is then applied to the study of guided waves and the transient response of layered superconducting tapes. These tapes are usually composed of layers of a superconducting material alternating between layers of a metallic material. The superconducting layers are orthotropic and in many cases are very thin with respect to the total thickness of the tapes. The most notable feature associated with the superconducting tapes is that the in-plane material properties of the superconducting layers are hard to measure. Three tape geometries are considered: a homogeneous nickel layer, a three-layered YBCO/nickel/YBCO and a three-layered nickel/YBCO/nickel. The total thickness of the YBCO layer is taken to be much smaller than that of the nickel layer. Our numerical studies show that even for this very thin superconducting layer, the dispersion and transient response in the last two cases are quite different from each other and from the homogeneous nickel layer. This is encouraging for ultrasonic characterization of in-plane material properties of thin superconducting inner or outer layers.

II. A GENERAL SOLUTION OF THE TRANSFORMED GREEN'S FUNCTIONS

In this section, an outline is given for calculating the Green's functions for a multilayered plate. Figure 1 shows a

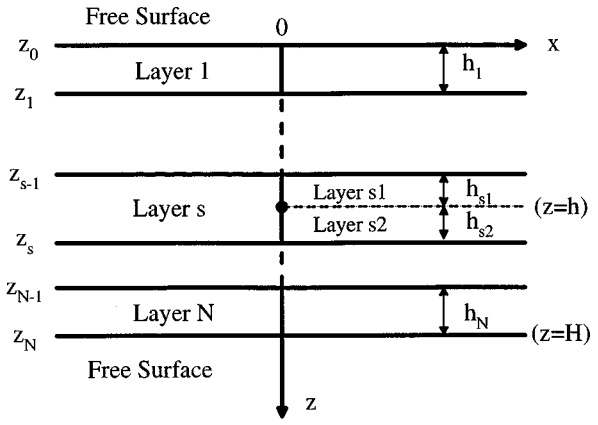

FIG. 1. Geometry of a multilayered superconducting plate under a concentrated line force.

multilayered superconducting plate made up of N parallel, homogeneous, and orthotropic layers. The layers are numbered serially with the layer at the top being layer 1 and the bottom being layer N. We place the Cartesian coordinates at the top free surface, and the z axis is drawn down into the medium. The jth layer is bounded by the interfaces $z=z_{j-1}$, z_j. Evidently, we have $z_0=0$ and $z_N=H$, where H is the total thickness of the layered plate. It is assumed that the symmetry axes of the layers are aligned parallel.

Consider a plane strain problem in the (x,z) plane. The equation of motion in each layer can then be described by

$$\sigma_{xx,x}+\sigma_{xz,z}+f_x=\rho\frac{\partial^2 u_x}{\partial t^2},$$
$$\sigma_{zx,x}+\sigma_{zz,z}+f_z=\rho\frac{\partial^2 u_z}{\partial t^2}, \tag{1}$$

with the constitutive relation given by

$$\begin{bmatrix}\sigma_{xx}\\ \sigma_{zz}\\ \sigma_{xz}\end{bmatrix}=\begin{bmatrix}c_{11} & c_{13} & 0\\ c_{13} & c_{33} & 0\\ 0 & 0 & c_{55}\end{bmatrix}\begin{bmatrix}u_{x,x}\\ u_{z,z}\\ u_{x,z}+u_{z,x}\end{bmatrix}. \tag{2}$$

In Eqs. (1) and (2), the density ρ, the body forces f_x and f_z, and the elastic constants c_{ij} are those belonging to the layer. They may differ from one layer to another.

In order to solve the governing equations in terms of the displacement, we first apply the Fourier transform with respect to time t

$$\begin{bmatrix}\overline{u}_x(x,z;\omega)\\ \overline{u}_z(x,z;\omega)\end{bmatrix}=\int_{-\infty}^{+\infty}\begin{bmatrix}u_x(x,z;t)\\ u_z(x,z;t)\end{bmatrix}e^{i\omega t}dt, \tag{3}$$

to Eqs. (1) and (2). This results in the following differential equations for the frequency-domain displacements:

$$c_{11}\overline{u}_{x,xx}+c_{13}\overline{u}_{z,zx}+c_{55}(\overline{u}_{x,zz}+\overline{u}_{z,xz})+\overline{f}_x=-\rho\omega^2\overline{u}_x,$$
$$c_{13}\overline{u}_{x,xz}+c_{33}\overline{u}_{z,zz}+c_{55}(\overline{u}_{x,zx}+\overline{u}_{z,xx})+\overline{f}_z=-\rho\omega^2\overline{u}_z. \tag{4}$$

Applying further another Fourier transform with respect to the horizontal variable x

$$\begin{bmatrix}U_x(k,z;\omega)\\ U_z(k,z;\omega)\end{bmatrix}=\int_{-\infty}^{+\infty}\begin{bmatrix}\overline{u}_x(x,z;\omega)\\ \overline{u}_z(x,z;\omega)\end{bmatrix}e^{-ikx}dx, \tag{5}$$

to Eq. (4), we then arrive at two ordinary differential equations for the double Fourier transformed displacements

$$-c_{11}k^2U_x+ikc_{13}U_{z,z}+c_{55}(U_{x,zz}+ikU_{z,z})+F_x=-\rho\omega^2U_x,$$
$$ikc_{13}U_{x,z}+c_{33}U_{z,zz}+c_{55}(ikU_{x,z}-k^2U_z)+F_z=-\rho\omega^2U_z, \tag{6}$$

where F_x and F_z are the double Fourier transformed force components. The general homogeneous solutions of the above equation for each layer can, therefore, be expressed as[6,10]

$$\begin{aligned}U_x(k,z;\omega)&=ik[(A_{11}\cosh r_1z-iA_{12}\sinh r_1z)\\ &\quad+b(A_{21}\cosh r_2z-iA_{22}\sinh r_2z)],\\ U_z(k,z;\omega)&=ar_1(A_{12}\cosh r_1z+iA_{11}\sinh r_1z)\\ &\quad+r_2(A_{22}\cosh r_2z+iA_{21}\sinh r_2z),\end{aligned} \tag{7}$$

where

$$\begin{aligned}a&=(\alpha k^2-k_2^2-r_1^2)/\delta r_1^2,\\ b&=(k_2^2-k^2+\beta r_2^2)/\delta k^2,\\ \alpha&=c_{11}/c_{55},\quad \beta=c_{33}/c_{55},\quad \delta=1+c_{13}/c_{55},\\ k_2&=\sqrt{\rho\omega^2/c_{55}},\end{aligned} \tag{8}$$

and r_1 and r_2 are the roots of the following equation:

$$(-\alpha k^2+r^2+k_2^2)(\beta r^2-k^2+k_2^2)+k^2r^2\delta^2=0. \tag{9}$$

Also, in Eq. (7), A_{11}, A_{12}, A_{21}, and A_{22} are constants.

III. GREEN'S FUNCTIONS IN THE FREQUENCY DOMAIN

In terms of the double Fourier transformed displacement solution (7), the transformed stresses can also be obtained. Furthermore, these solutions for each layer (say layer j) can be expressed in terms of a propagating relation as

$$[Q(z_j)]=[P_j(z_j-z_{j-1})][Q(z_{j-1})]. \tag{10}$$

Here, the solution $[Q]$ at the top interface z_{j-1} of layer j is related to that at the bottom interface z_j by the propagator matrix $[P_j]$ of the layer. While the elements of the propagator matrix are given in the appendix, the solution column matrix is defined as

$$[Q]=\{U_x,U_z,T_{zz},T_{xz}\}^t, \tag{11}$$

with T_{zz} and T_{xz} being the double Fourier transformed stress components obtained by

$$\overline{\sigma}_{lm}(x,z;\omega)=\int_{-\infty}^{\infty}\sigma_{lm}(x,z;t)e^{i\omega t}dt,$$
$$T_{lm}(k,z;\omega)=\int_{-\infty}^{+\infty}\overline{\sigma}_{lm}(x,z;\omega)e^{-ikx}dx. \tag{12}$$

Suppose now that there is a line force with time history $f(t)$ located on the z axis at the depth $z=h$ which belongs to layer s (Fig. 1), i.e.,

$$f_m(x,z;t)=\delta(x)\,\delta(z-h)f(t)n_m, \tag{13}$$

where n_m are the components of the unit force vector in the coordinate axes.

The double Fourier transform of this line force is

$$F_m(k,z;\omega)=\delta(z-h)F(\omega)n_m, \tag{14}$$

with $F(\omega)$ being the frequency-domain behavior of $f(t)$. It is easy to show that the traction discontinuity caused by the line force is

$$\begin{aligned}\Delta T_{xz}&\equiv T_{xz}(h+0)-T_{xz}(h-0)=F(\omega)n_x,\\ \Delta T_{zz}&\equiv T_{zz}(h+0)-T_{zz}(h-0)=F(\omega)n_z.\end{aligned} \tag{15}$$

For handling the propagation of the matrix $[P_j]$, we artificially divide the source layer s into two sublayers $s1$ and $s2$ (Fig. 1). Using then the propagating relation (10) and the discontinuity condition (15), we found that[12]

$$\begin{aligned}&[Q(z_N)]-[P_N][P_{N-1}]\cdots[P_1][Q(z_0)]\\ &\quad=[P_N][P_{N-1}]\cdots[P_{s2}][\Delta Q],\end{aligned} \tag{16}$$

with

$$[\Delta Q]=\{0,0,-F(\omega)n_x,-F(\omega)n_z\}^t. \tag{17}$$

Now, substituting the free-traction boundary conditions at the top (z_0) and bottom (z_N) surfaces into Eq. (16), we can solve the Green's displacement in the double Fourier transformed domain at either the top or bottom surface. For example, for a line force in the x direction, the Green's displacement at the top surface is derived as

$$\begin{bmatrix}U_x(k,z_0;\omega)\\ U_z(k,z_0,\omega)\end{bmatrix}=\frac{F(\omega)}{a_{31}a_{42}-a_{41}a_{32}}\begin{bmatrix}b_{34}a_{42}-b_{44}a_{32}\\ a_{31}b_{44}-a_{41}b_{34}\end{bmatrix}. \tag{18}$$

Similarly, for a line force in the z direction, it is

$$\begin{bmatrix}U_x(k,z_0;\omega)\\ U_z(k,z_0;\omega)\end{bmatrix}=\frac{F(\omega)}{a_{31}a_{42}-a_{41}a_{32}}\begin{bmatrix}b_{33}a_{42}-b_{43}a_{32}\\ a_{31}b_{43}-a_{41}b_{33}\end{bmatrix}. \tag{19}$$

In Eqs. (18) and (19)

$$\begin{aligned}[a]&=[P_N][P_{N-1}]\cdots[P_1],\\ [b]&=[P_N][P_{N-1}]\cdots[P_{s2}].\end{aligned} \tag{20}$$

Having obtained the surface displacements, the propagating relation (10) can then be used again to find the solution at any vertical level. For example, for $z_{j-1}\leqslant z\leqslant z_j$, we have

$$[Q(z)]=[P_j(z-z_{j-1})][P_{j-1}]\cdots[P_1][Q(z_0)]. \tag{21}$$

It is well known that overflow may occur in the high-frequency region due to the multiplication of the propagator matrix $[P_j]$. This problem is avoided by the direct propagator matrix method proposed by Pan.[12]

In order to get the frequency-domain solutions, we need to carry out the inverse transform of Eq. (5). Here, we use Cauchy's residue theorem to evaluate these integrals, which converts the integral into a residue summation in the suitable domain. For example, for the displacement component in the x direction and for $x\geqslant 0$, this integral can be expressed as[9]

$$\begin{aligned}\overline{u}_x(x,z;\omega)&=\frac{1}{2\pi}\int_{-\infty}^{+\infty}U_x(k,z;\omega)e^{ikx}dk\\ &=-i\sum_{m=1}^{M}U_x(k_m,z;\omega)\exp(ik_mx).\end{aligned} \tag{22}$$

The poles in Eq. (22) are actually the roots of the dispersion equation

$$a_{31}a_{42}-a_{41}a_{32}=0. \tag{23}$$

These roots can be found accurately by the method described in Zhu, Shah, and Datta[6] and Pan *et al.*[11] Since all the poles are of first order, the residue summation can be carried out exactly by finding the exact derivative of the left-hand side of Eq. (23) with respect to the wave-number k. For a given frequency, there are only a finite number of propagating modes; all other modes are nonpropagating and decay exponentially to zero in the selected half plane of k, when $|k|$ approaches infinity. Therefore, the finite number M in Eq. (22) will be enough to give an accurate result, with a suitable range being $40\leqslant M\leqslant 60$.

In the actual calculation, we first use the stiffness-based Rayleigh–Ritz technique to find the approximate values of the complex wave numbers. Then, the Muller's method is employed to the exact dispersion Eq. (23) to calculate the exact poles. Once these poles are found, Eq. (22) or the like is used to find the Green's functions in the frequency domain. It should be emphasized here that for a given frequency, we need to find the poles only once. With these poles, the frequency-domain Green's functions for any pair of source and field points can be evaluated accurately using the direct propagator matrix method, which is therefore very efficient.

IV. GREEN'S FUNCTIONS IN THE TIME DOMAIN

To obtain the time-domain response, the inverse transform of Eq. (3) needs to be carried out. For example, the time-domain displacements $u_x(t)$ and $u_z(t)$ can be expressed as

$$\begin{bmatrix}u_x(x,z;t)\\ u_z(x,z;t)\end{bmatrix}=\frac{1}{2\pi}\int_{-\infty}^{+\infty}\begin{bmatrix}\overline{u}_x(x,z;\omega)\\ \overline{u}_z(x,z;\omega)\end{bmatrix}F(\omega)e^{-i\omega t}d\omega. \tag{24}$$

Again, $F(\omega)$ is the Fourier transform of the time dependence of the line force $f(t)$. The integration involved in Eq. (24) is usually carried out numerically. For an infinite plate, however, difficulties with the integration may occur due to the singularity of the frequency-domain solution at $\omega=0$ and at the cutoff frequencies $(k=0)$. To overcome these difficul-

TABLE I. Geometry and material properties of the homogeneous nickel plate.

Layer	Thickness (μm)	Density (10^3 kg/m^3)	c_{11} (GPa)	c_{13} (GPa)	c_{33} (GPa)	c_{55} (GPa)
Nickel	100	8.910	298.95	129.53	298.95	84.71

TABLE II. Geometry and material properties of the three-layered YBCO/Ni/YBCO plate.

Layer	Thickness (μm)	Density (10^3 kg/m^3)	c_{11} (GPa)	c_{13} (GPa)	c_{33} (GPa)	c_{55} (GPa)
YBCO	5	6.333	268	95	186	49
Nickel	100	8.910	298.95	129.53	298.95	84.71
YBCO	5	6.333	268	95	186	49

ties, a small imaginary part of the frequency ω can be introduced into the integrand of Eq. (24).[9,13,14] By doing so, Eq. (24) can be written equivalently as

$$\begin{bmatrix} u_x(x,z;t) \\ u_z(x,z;t) \end{bmatrix} = \frac{e^{\eta t}}{2\pi} \int_{-\infty}^{+\infty} \begin{bmatrix} \overline{u_x}(x,z;\omega+i\eta) \\ \overline{u_z}(x,z;\omega+i\eta) \end{bmatrix} \times F(\omega+i\eta) e^{-i\omega t} d\omega, \tag{25}$$

where

$$F(\omega+i\eta) = \int_0^{t_d} e^{-\eta t} f(t) e^{i\omega t} dt, \tag{26}$$

in which t_d is the duration of the line force and η is the shifting constant. For the numerical examples presented in the next section, the normalized η is chosen to be 0.1, as in Liu and Achenbach.[9]

V. NUMERICAL EXAMPLES

We now apply this formulation to three cases: a homogeneous plate made of nickel (named case I, see Table I), a three-layered superconducting plate made of YBCO, nickel, and YBCO (named case II, i.e., YBCO/Ni/YBCO, see Table II), and a three-layered superconducting plate made of nickel, YBCO, and nickel (named case III, i.e., Ni/YBCO/Ni, see Table III). YBCO is orthotropic with elastic properties being taken from Lei *et al.*,[15] and is such that the x and z axes are along the maximum and minimum of its elastic constants c_{ij}.

As we mentioned earlier, Eq. (23) is actually the dispersion relation for the layered plate. Therefore, as a by-product, Eq. (23) can be used to find the dispersion behavior of the layered plate. For instance, Figs. 2(a) and 2(b) show the comparison of the dispersion curves for cases I and II and for cases I and III. In Figs. 2(a) and 2(b), the normalized wave number is $k' = kH_I$, where H_I is the thickness of nickel, and the normalized frequency is $\omega' = \omega H_I / c_s$, where c_s is the shear velocity in nickel. It is observed clearly that even for a very thin YBCO layer either on both sides of the nickel layer (case II, YBCO/Ni/YBCO), or in the middle of it (case III, Ni/YBCO/Ni), the dispersion behaviors of the homogeneous nickel plate and the superconducting tapes are significantly different. In particular, the cutoff frequencies for both superconducting tapes (cases II and III) are quite different from those of the nickel, as listed in Table IV. Addition of the superconducting YBCO layer is, in general, to lower the cutoff frequency. It is also noteworthy that for the nickel plate, the cutoff frequencies calculated by our numerical method are very close to the exact values, which are either $n\pi$ or $n\pi c_l / c_s$ ($n = 1,2,3,...$), with c_l being the longitudinal velocity in the nickel plate (Table IV).

When comparing the cutoff frequencies of cases II and III (Table IV), we note that for the same mode, the cutoff frequency of case III (Ni/YBCO/Ni) is either lower than or

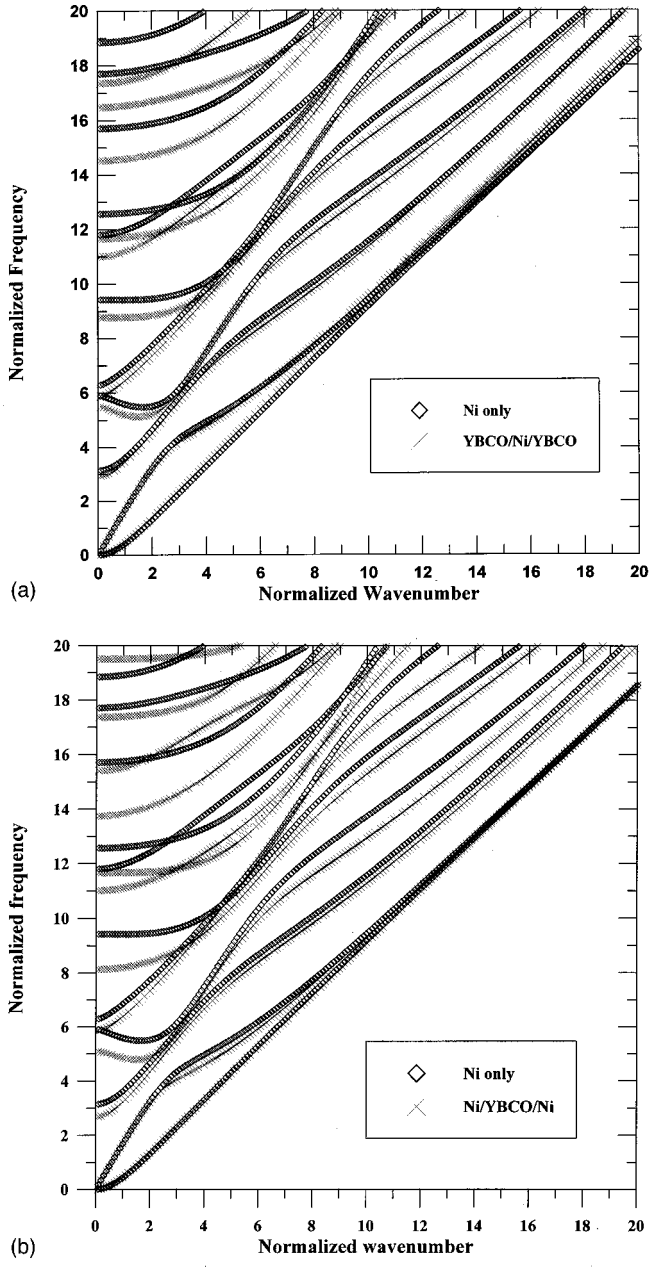

FIG. 2. (a) Comparison of dispersion curves for a homogenous nickel plate and a three-layered YBCO/Ni/YBCO plate. (b) Comparison of dispersion curves for a homogenous nickel plate and a three-layered Ni/YBCO/Ni plate.

TABLE III. Geometry and material properties of the three-layered Ni/YBCO/Ni plate.

Layer	Thickness (μm)	Density (10^3 kg/m^3)	c_{11} (GPa)	c_{13} (GPa)	c_{33} (GPa)	c_{55} (GPa)
Nickel	50	8.910	298.95	129.53	298.95	84.71
YBCO	10	6.333	268	95	186	49
Nickel	50	8.910	298.95	129.53	298.95	84.71

TABLE IV. Comparison of cutoff frequencies for nickel, YBCO/Ni/YBCO, and Ni/YBCO/Ni plates.

Nickel (Exact)	Nickel (Numer.)	YBCO/Ni/YBCO	Ni/YBCO/Ni
$\pi = 3.14\ 592\ 65$	3.141 592 65	2.932 101 64	2.682 612 24
$\pi c_1/c_s = 5.901\ 763\ 62$	5.901 763 63	5.508 444 12	5.090 639 22
$2\pi = 6.283\ 185\ 31$	6.283 185 31	5.858 054 96	5.858 054 96
$3\pi = 9.424\ 777\ 96$	9.424 777 96	8.771 366 24	8.131 763 95
$2\pi c_1/c_s = 11.803\ 52\ 72$	11.803 527 3	11.006 748 01	11.006 748 01
$4\pi = 12.566\ 370\ 6$	12.566 370 6	11.664 931 29	11.664 931 29
$5\pi = 15.707\ 963\ 3$	15.707 963 3	14.531 004 67	13.749 529 22
$3\pi c_1/c_s = 17.705\ 290\ 9$	17.705 290 9	16.484 325 76	15.399 567 10
$6\pi = 18.849\ 555\ 9$	18.849 555 9	17.361 707 11	17.361 707 11

exactly equal to that of case II (YBCO/Ni/YBCO). The corresponding modes for which the cutoff frequencies are the same for both cases are the symmetrical modes with an even multiplier of π. Even though the cutoff frequencies are quite different for the three cases, the modal displacements are very similar to each other. For example, Figs. 3(a) and 3(b) show the modal displacement $\mathrm{Re}(u_x)$ for a_0 when $\omega' = 7$ and 14, respectively, where the vertical coordinate z has been shifted so that $z = 0$ is the symmetrical plane of the layered plates. It is noted that the modal shapes are all similar except for case III where the thin soft middle layer of YBCO behaves like an interface layer.[16–18] It should be emphasized that in both cases II and III, the total thickness of the YBCO layer is the same. But the dispersions in these two cases are quite different. It is not apparent that this can be explained by some simple scaling of the thickness.

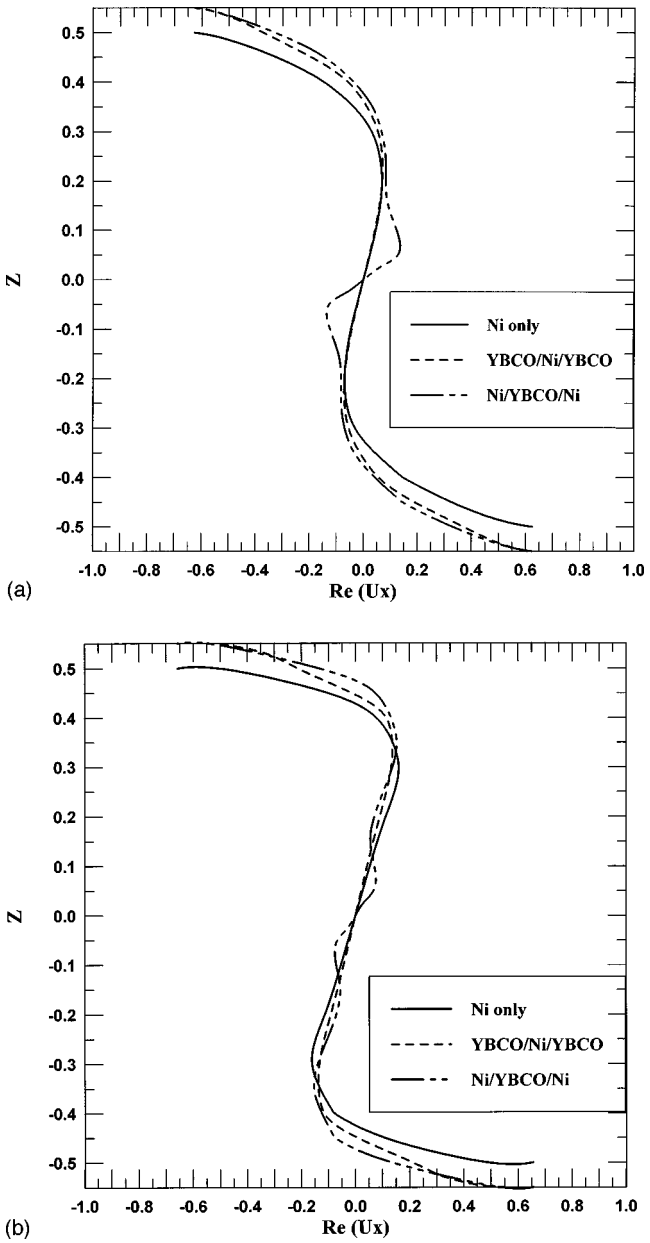

FIG. 3. Modal displacement $\mathrm{Re}(u_x)$ for branch No. 1(a_0) for $\omega' = 7$ (a) and $\omega' = 14$ (b).

With the calculated wave numbers for given frequencies, the response of a layered plate to a line force in the frequency domain can be evaluated accurately. For example, Fig. 4 shows the amplitude variation of the frequency-domain Green's displacements u_x and u_z along the top free surface of a homogeneous plate caused by a vertical time–harmonic line load with unit amplitude applied at the origin (0, 0). The plate has a thickness of H and a Poisson's ratio of 1/3. The normalized frequency for this example is fixed at $\omega H/c_s = 3.14$. Liu and Achenbach[9] used the strip-element method to calculate the amplitude of u_z. It is noted that the result for u_z is very close to that in Liu and Achenbach.[9]

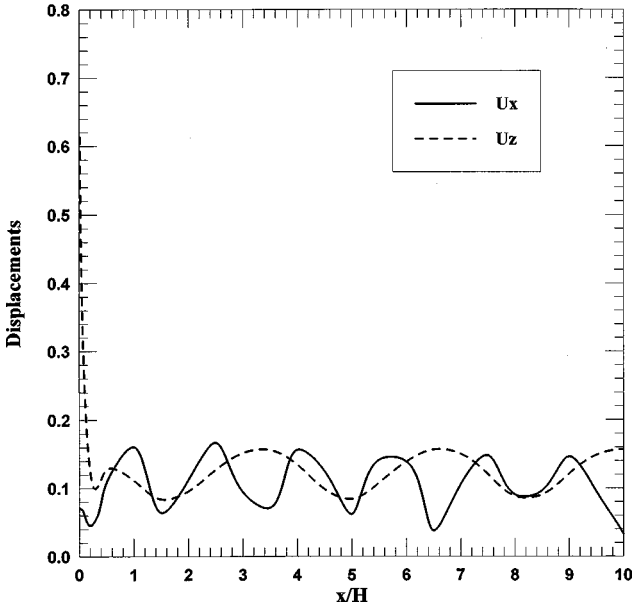

FIG. 4. Frequency-domain Green's displacements (at $\omega' = 3.14$) on the top surface of an isotropic plate subjected to a vertical time–harmonic line load at the origin (0,0).

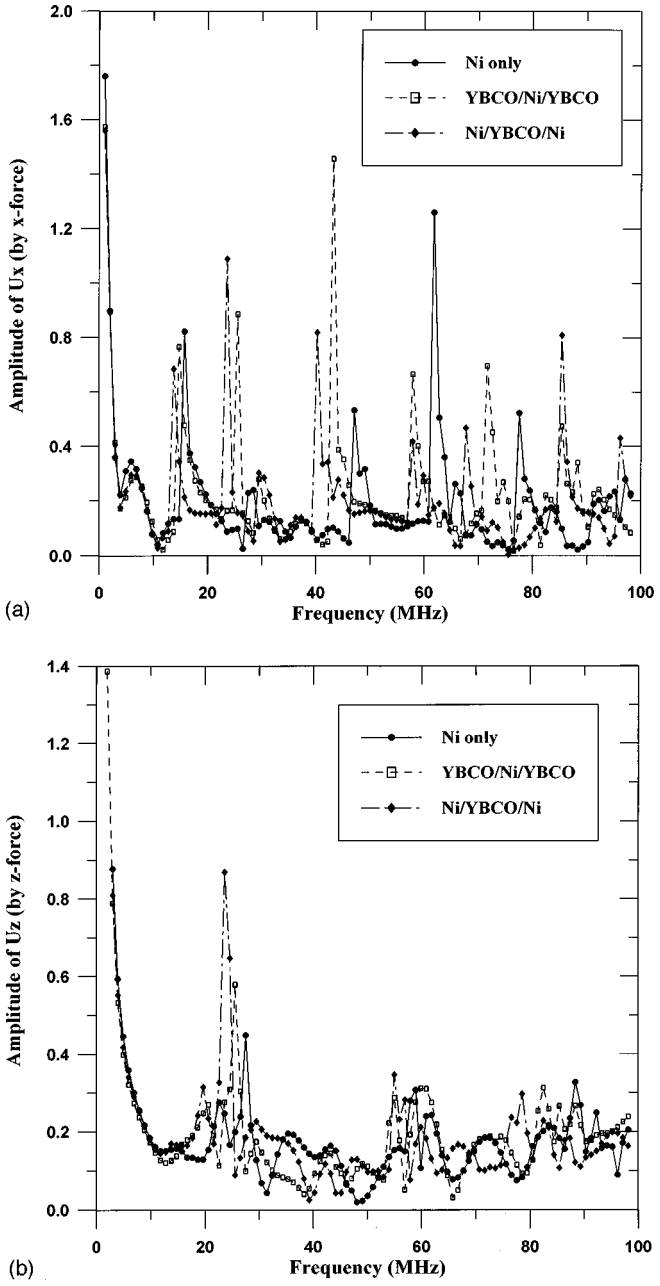

FIG. 5. Frequency-domain Green's displacements at $(10H_I,0)$ caused by a line force at (0,0): u_x in (a) due to a line force in the x direction, and u_z in (b) due to a line force in the z direction.

Now, the method is used to calculate the Green's functions over a certain frequency range for a given observation point. As an example, Figs. 5(a) and 5(b) are the calculated spectra of u_x caused by a line force in the x direction, and that of u_z caused by a line force in the z direction. The loading is at the origin (0,0) and the response is calculated at the top surface of the layered plate at a horizontal distance of $10H_I$, where H_I is again the total thickness of the nickel layer. As can be observed, the spectra for the three cases considered are quite different. The sharp peak amplitudes corresponding to the cutoff frequencies are found to be shifted and correspond to those listed in Table IV. The frequency spectra can be used to characterize the properties.

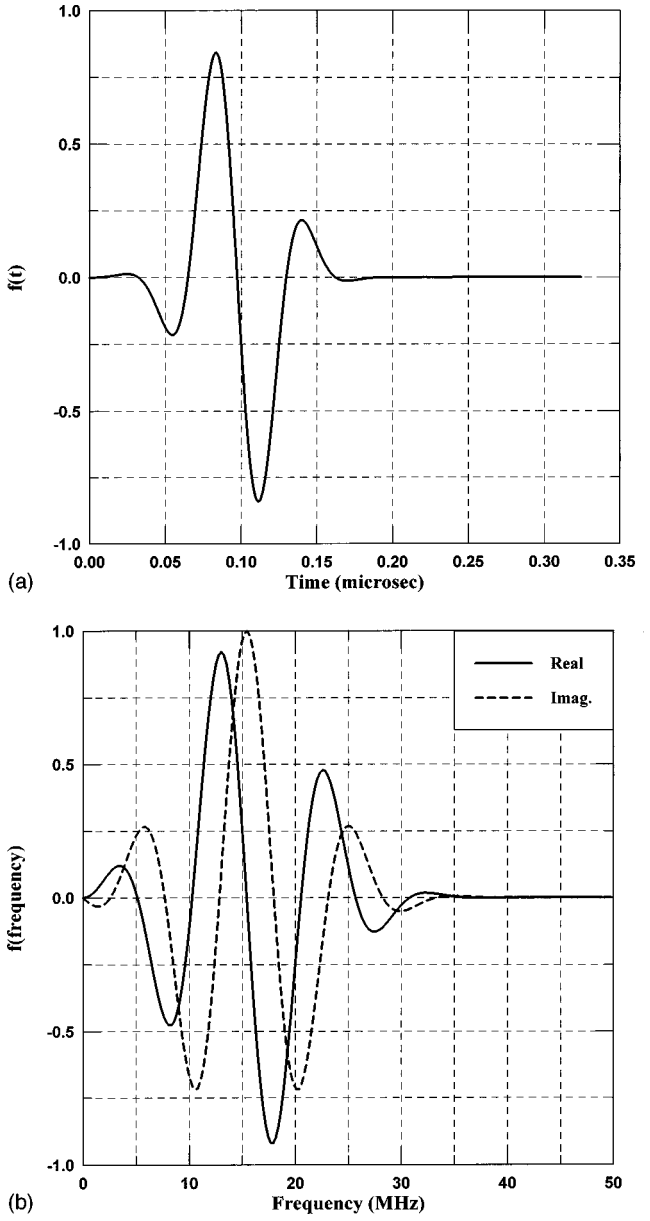

FIG. 6. Time history of the applied load in (a) and its frequency-domain behavior in (b).

In order to calculate the time-domain Green's functions, a time history of the line force has been assumed. Here, a Gaussian-type behavior is chosen with the expression of[8,9]

$$f(t)=\frac{2}{\sigma\sqrt{2\pi}}\exp\left[-\frac{(t-t_0)^2}{2\sigma^2}\right]\sin(\omega_c t),\quad 0\leqslant t\leqslant t_d, \tag{27}$$

where σ is a parameter controlling the width of the pulse, t_0 determines the time delay of the pulse, and ω_c is the center angular frequency of the pulse. As an example, we chose $\sigma=0.8$, $t_0=3.0H_I/c_s$, and $\omega_c=3.14c_s/H_I$, where H_I and c_s are, respectively, the thickness of and shear velocity in the isotropic layer. For these fixed parameters, the time and frequency dependencies of the line force are shown, respectively, in Figs. 6(a) and 6(b). It is seen from the frequency

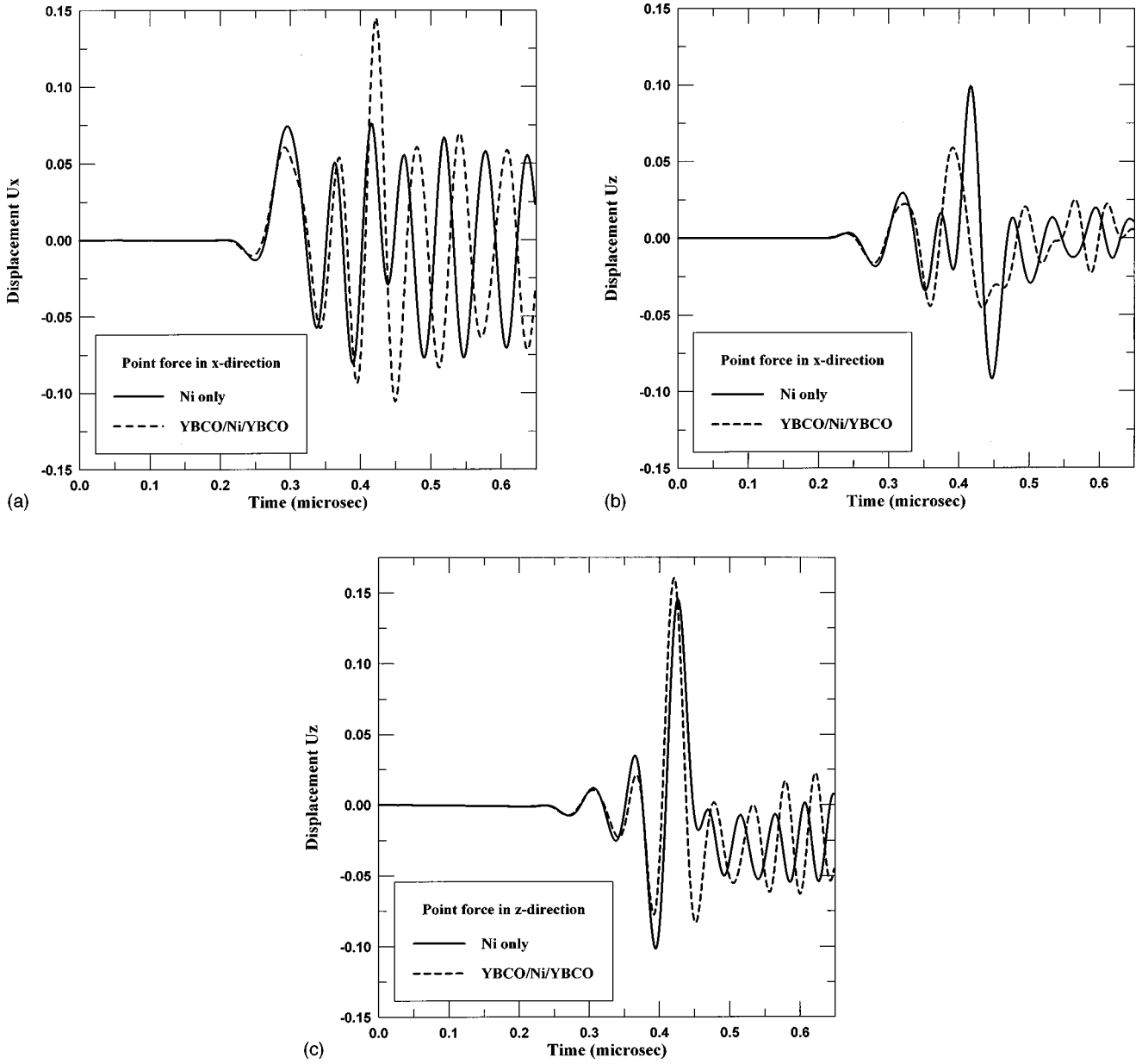

FIG. 7. Time-domain Green's displacements for a homogenous nickel plate and a three-layered YBCO/Ni/YBCO plate. While the field point is at $(10H_1,0)$, the source point is at the origin (0,0): $u_x(t)$ in (a) due to a line force in the x direction, $u_z(t)$ in (b) due to a line force in x direction, and $u_z(t)$ in (c) due to a line force in z direction.

dependence of the line force that the amplitude approaches zero after a frequency greater than 40 MHz. Therefore, the high frequencies are filtered out.

While Figs. 7(a)–7(c) show the comparison of the time-domain Green's functions in the nickel and three-layered YBCO/Ni/YBCO plates, Figs. 8(a)–8(c) show the comparison of the time-domain Green's functions in the nickel and three-layered Ni/YBCO/Ni plates. Again, the geometry and material properties are given in Tables I–III. As in Fig. 5, the observation point is at $(10H_1,0)$ and the source point is at the origin (0,0). While Figs. 7(a) and 8(a) and 7(b) and 8(b) show the Green's displacements $u_x(t)$ and $u_z(t)$ caused by the x-direction force, Figs. 7(c) and 8(c) show the Green's displacement $u_z(t)$ caused by the z-direction force. The Green's displacement $u_x(t)$ due to the z-direction force is exactly opposite to the Green's displacement $u_z(t)$ due to the x-direction force, a consequence of the Betti's reciprocal theorem. As can be observed clearly, the time-domain responses of the nickel, YBCO/Ni/YBCO, and Ni/YBCO/Ni plates are significantly different. It is noted that the high peaks of $u_z(t)$ in Figs. 7(c) and 8(c) correspond to the Rayleigh waves in the nickel, YBCO/Ni/YBCO, and Ni/YBCO/Ni plates. While the Rayleigh wave in the nickel arrives at 0.455 μs, the Rayleigh waves in YBCO/Ni/YBCO and Ni/YBCO/Ni arrive at 0.422 μs and 0.433, respectively. Based on the information in Figs. 7(c) and 8(c) and taking account of the delayed time 0.083 μs in the time history of the applied load, we obtained the Rayleigh velocities of $0.940c_s$, $0.957c_s$, and $0.927c_s$, respectively, for the nickel, YBCO/Ni/YBCO, and Ni/YBCO/Ni plates. These values are

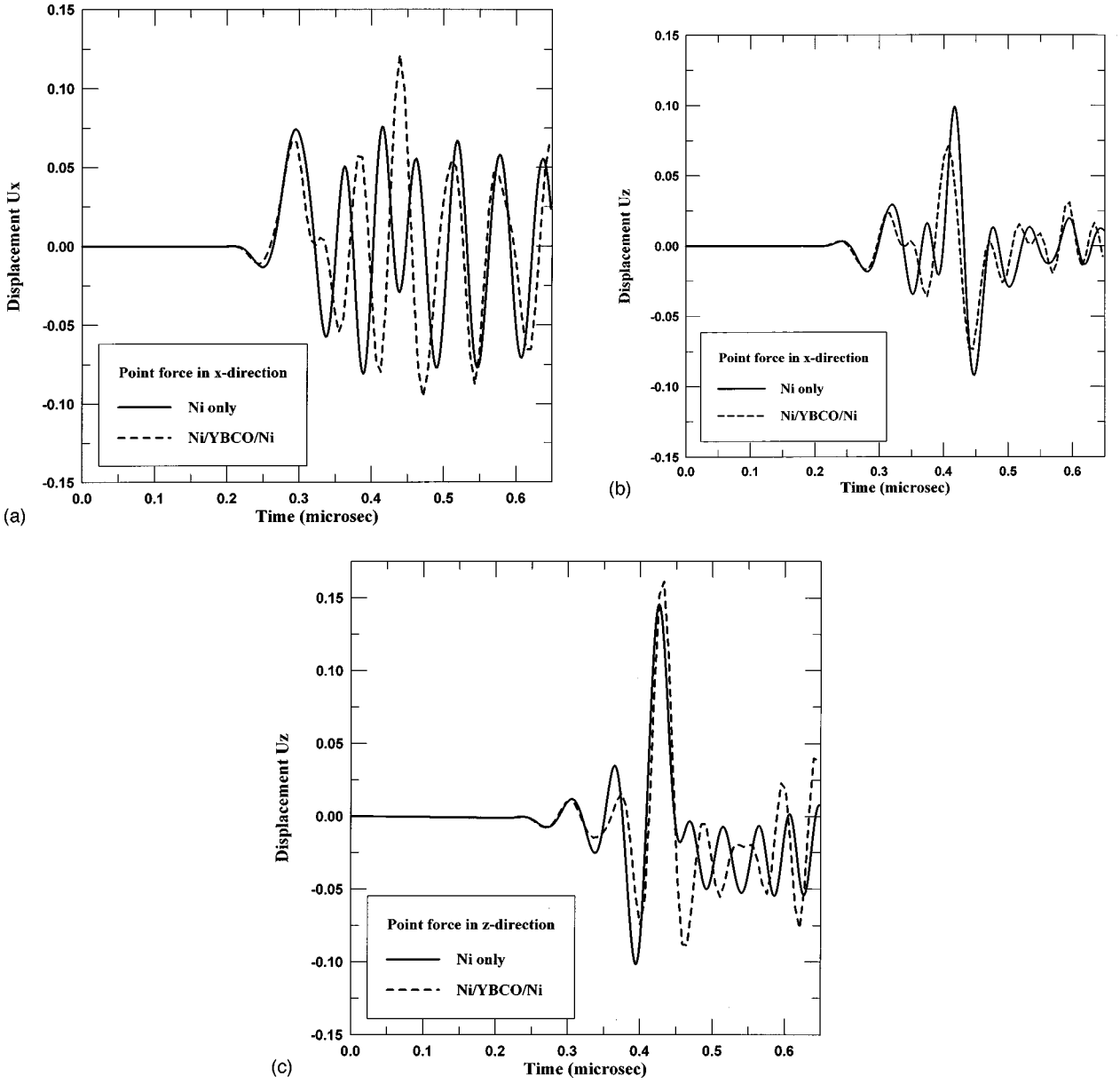

FIG. 8. Time-domain Green's displacements for a homogenous nickel plate and a three-layered Ni/YBCO/Ni plate. While the field point is at $(10H_l,0)$, the source point is at the origin (0,0): $u_x(t)$ in (a) due to a line force in the x direction, $u_z(t)$ in (b) due to a line force in x direction, and $u_z(t)$ in (c) due to a line force in z direction.

close to $0.929c_s$, $0.947c_s$, and $0.926c_s$ calculated from the slopes of the first two branches of the dispersion curves shown in Figs. 2(a) and 2(b) as $k\rightarrow\infty$. It is noted that for the homogeneous nickel case, the Rayleigh velocity obtained from our calculation is close to the approximate value of $0.927c_s$ derived from the relation between the Rayleigh wave velocity and the Poisson's ratio.[19]

VI. CONCLUSION

We presented an analytical method for calculating the elastodynamic Green's functions in two-dimensional (plane strain) layered anisotropic plates. We first expressed the frequency-domain solution by the residue theorem with poles being evaluated by the Muller's method. Initial estimates of these poles are found using a stiffness-based Rayleigh–Ritz technique and are refined using the exact dispersion relation derived by the direct propagator matrix method. The time-domain solution was obtained by the inverse Fourier transform technique combined with the exponential window method. The formulation is then applied to the study of dispersion of the guided waves and transient response of the layered tapes: a homogeneous plate made of nickel, a three-layered superconducting tape made of YBCO/Ni/YBCO, and a three-layered superconducting tape made of Ni/YBCO/Ni. In the last two cases, attention has been focused on the small thickness of the YBCO layer. It is found that the dispersion behaviors and the time-domain responses are significantly different in the three-layered cases, even though the superconducting layer YBCO is very thin as compared to the total thickness of the tape. These differences in their responses could be used for the ultrasonic characterization of the in-plane material properties of the superconducting layers. Al-

though the study was limited to the plane strain case, it is possible to extend the technique to study the three-dimensional response due to a point load. For that general case, it would be necessary to obtain the frequency-wave-number relation for waves propagating at an arbitrary angle to the x axis. Zhu[20] reported the result of some limited investigation for low frequencies. Investigation of the high-frequency response is under way and will be reported in the future.

ACKNOWLEDGMENTS

The authors would like to thank R. Sesselmann, Dr. M. Dunn, and Dr. A. J. Niklasson of the Department of Mechanical Engineering at CU-Boulder for many helpful discussions. The work presented in this article is partially supported by the Division of Basic Energy Sciences, Department of Energy under Grant No. DE-FG03-97ER14738.

APPENDIX

The elements of the propagator matrix $[P_j]$ of layer j are

$$(1,1)=\frac{ikc_{55}}{\Delta_1}(dchr_1h-cbchr_2h),$$

$$(2,1)=\frac{c_{55}}{\Delta_1}(r_1adshr_1h-r_2cshr_2h),$$

$$(3,1)=\frac{cdc_{55}^2}{\Delta_1}(chr_1h-chr_2h),$$

$$(4,1)=\frac{ikc_{55}^2}{\Delta_1}[r_1d(1+a)shr_1h-r_2c(1+b)shr_2h],$$

$$(1,2)=\frac{k^2c_{55}}{\Delta_2}[r_2(1+b)shr_1h-r_1b(1+a)shr_2h],$$

$$(2,2)=\frac{ikr_1r_2c_{55}}{\Delta_2}[-a(1+b)chr_1h+(1+a)chr_2h],$$

$$(3,2)=\frac{ikc_{55}^2}{\Delta_2}[-r_2c(1+b)shr_1h+r_1d(1+a)shr_2h],$$

$$(4,2)=\frac{r_1r_2(1+a)(1+b)k^2c_{55}^2}{\Delta_2}(chr_1h-chr_2h),$$

$$(1,3)=\frac{bk^2}{\Delta_1}(chr_1h-chr_2h),$$

$$(2,3)=\frac{ik}{\Delta_1}(-r_1abshr_1h+r_2shr_2h),$$

$$(3,3)=\frac{ikc_{55}}{\Delta_1}(-cbchr_1h+dchr_2h),$$

$$(4,3)=\frac{k^2c_{55}}{\Delta_1}[r_1b(1+a)shr_1h-r_2(1+b)shr_2h],$$

$$(1,4)=\frac{ik}{\Delta_2}[r_2shr_1h-r_1abshr_2h],$$

$$(2,4)=\frac{ar_1r_2}{\Delta_2}[chr_1h-chr_2h],$$

$$(3,4)=\frac{c_{55}}{\Delta_2}(r_2cshr_1h-r_1adshr_2h),$$

$$(4,4)=\frac{ikr_1r_2c_{55}}{\Delta_2}[(1+a)chr_1h-a(1+b)chr_2h].$$

In these expressions

$$c=(1-\delta)k^2+\beta ar_1^2,\quad d=(1-\delta)bk^2+\beta r_2^2,$$

$$\Delta_1=ik\beta c_{55}(r_2^2-abr_1^2),\quad \Delta_2=ikc_{55}r_1r_2(1-ab),$$

$$h=z_j-z_{j-1},\quad i=\sqrt{-1}.$$

[1] T. Kundu and A. K. Mal, Wave Motion **7**, 459 (1985).
[2] A. K. Mal, Wave Motion **10**, 257 (1988).
[3] T. H. Ju, Ph.D. thesis, University of Colorado at Boulder, CO (1991).
[4] G. Waas, Ph.D. thesis, University of California at Berkeley, CA (1972).
[5] E. Kausel, Technical Report No. R81-13, Department of Civil Engineering, M.I.T., Cambridge, MA (1981).
[6] J. Zhu, A. H. Shah, and S. K. Datta, J. Eng. Mech. **121**, 26 (1995).
[7] J. Zhu, A. H. Shah, and S. K. Datta, Int. J. Numer. Methods Eng. **39**, 1017 (1996).
[8] J. Zhu and A. H. Shah, Int. J. Solids Struct. **34**, 1719 (1997).
[9] G. R. Liu and J. D. Achenbach, J. Appl. Mech. **62**, 607 (1995).
[10] W. M. Karunasena, A. H. Shah, and S. K. Datta, Int. J. Solids Struct. **27**, 949 (1991).
[11] E. Pan, J. Rogers, S. K. Datta, and A. H. Shah, Mech. Mater. **31**, 165 (1999).
[12] E. Pan, Appl. Math. Modelling **21**, 509 (1997).
[13] N. Vasudevan and A. K. Mal, J. Appl. Mech. **52**, 356 (1985).
[14] E. Kausel and J. M. Roesset, J. Eng. Mech. **118**, 721 (1992).
[15] M. Lei, J. L. Sarrao, W. M. Visscher, T. M. Bell, J. D. Thompson, A. Migliori, U. W. Welp, and B. W. Veal, Phys. Rev. B **47**, 6154 (1993).
[16] S. K. Datta, A. H. Shah, W. Karunasena, P. Olsson, and A. Bostrom, Mater. Sci. Eng., A **126**, 141 (1990).
[17] P. C. Xu and S. K. Datta, J. Appl. Phys. **67**, 6779 (1990).
[18] T. H. Ju and S. K. Datta, J. Nondestruct. Eval. **11**, 227 (1992).
[19] J. D. Achenbach, *Wave Propagation in Elastic Solids* (North-Holland, New York, 1976).
[20] J. Zhu, Ph.D. thesis, University of Manitoba, Manitoba, Canada (1996).